International Journal of Humanoid Robotics

Compliance Control and Human-Robot Interaction: Part II - Experimental Examples

Said G Khan

Department of Mechanical Engineering,
College of Engineering Yanbu,
Taibah University, Saudi Arabia and Bristol Robotics Laboratory, UWE and UOB, UK *
engr_ghani@hotmail.com

Guido Herrmann

Bristol Robotics Lab (BRL) and Mechanical Engineering Department, University of Bristol
Bristol, UK
g.herrmann@Bristol.ac.uk

Alexander Lenz

Bristol Robotics Laboratory, University of the West of England, Bristol, UK

Mubarak Al Grafi

Taibah University, AL Madinah, Saudi Arabia

Tony Pipe

Bristol Robotics Laboratory, University of the West of England, Bristol, UK

Chris Melhuish

Bristol Robotics Laboratory, University of Bristol and University of the West of England,
Bristol, UK

Received Day Month Year
Revised Day Month Year
Accepted Day Month Year

Compliance control is highly relevant to human safety in human robot interaction (HRI). This paper presents multi-dimensional compliance control of a humanoid robot arm. A dynamic model-free adaptive controller with an anti-windup compensator is implemented on four degrees of freedom of a humanoid robot arm. The paper is aimed to compliment the associated review paper on compliance control. This is a model reference adaptive compliance scheme which employs end-effector forces (measured via joint torque sensors) as a feedback. The robot's body-own torques are separated from external torques via a simple but effective algorithm. In addition, an experiment of physical human robot interaction is conducted employing the above mentioned adaptive compliance control

*Taibah University College of Engineering Yanbu, Al Madinah, Saudi Arabia.

along with a speech interface. The experiment is focused on passing an object (a cup) between a human and a robot. Compliance is providing an immediate layer of safety for this HRI scenario by avoiding pushing, pulling or clamping and minimizing the effect of collisions with the environment.

Keywords: Compliance; Impedance ; Humanoids; Optimal Adaptive Control; HRI; pHRI

1. Introduction

Human safety is in the core of human-robot cooperation and physical human-robot interaction (pHRI). Compliance control can help in achieving safe human-robot interaction. There are two options for compliance, passive compliance and active compliance. Passive compliance is based on a suitable robot mechanical build, which avoids physical injury at impact or due to other interacting forces. However, passive compliance cannot be used in our case. This is due to the fact that our BERT II robotic arm is inherently rigid.

In our case, active compliance control scheme has therefore been used to make it safer for interaction with humans. The torque sensors installed in the robot joints have been used to implement the scheme. Active compliance has been investigated by various researchers to deal with the safety aspects of human-robot interaction. Some of the related work can be found in [20,26,27,1,3,33,38,5,37].

Often compliance or impedance controllers are model-based nonadaptive schemes, e.g. [4] [5] [27] [25] [2] [3] and [19]. However, for a large scale multi-redundant robot system, exact identification is rather complex. Component ageing or damage may invalidate these dynamics identifications. Hence, it is preferred here to use adaptive schemes which can guarantee predesigned passive characteristics in the face of a changing system. Further details on recent developments in compliance control are given in the associated review paper, Part I.

In general, there are two main types of adaptive control schemes i.e. *model reference adaptive control (MRAC)* and *self tuning (ST)* adaptive control. In MRAC, the adaptation mechanism is looking for suitable parameters, so that the plant response becomes the same as that of the reference model (see [28]). The reference model in our case is a second order mass-spring-damper system. Compliance control research for safe HRI has attracted many researchers recently e.g. [6,10,31,] [34] [21,35,] [36].

In the next section, MRAC based model reference adaptive compliance control with anti-windup compensation and posture control scheme is introduced, followed by the implementation (in real-world experiment) on a humanoid robot arm [16,15]. The Cartesian (x, y and z) tracking scheme for 4 DOFs (using shoulder flexion, shoulder abduction, humeral rotation and elbow flexion joints of the BERT II arm shown in Figure 1 (a)) is tested for multi-dimensional compliance control using the robot's joint torque sensors. For multi-dimensional compliance control of the arm, the robot's body-own torques need to be separated from the external torques. Hence, initially, for a couple of minutes, a recursive least square algorithm is run to learn the robot's body-own torques due to gravity and then the learnt parameters of this body torque estimators are kept and normal operation of the control begins.

These body torque estimators are used to find the external torques, by subtracting robot's body-own torques estimates from the sensor measured torques. Followed by an HRI experimental example (Section, 4) using this Compliance control scheme along with a separate control scheme for grasping incorporating speech (human-robot verbal communication). The HRI experiment is included as an application for the compliance controller presented in the previous section. The passing of an object between a human and a robot is performed while communicating through speech and employing the compliance controller for safety [14].

2. Multi-Dimensional Adaptive Compliance Control of BERT II Arm

In this section, a model reference adaptive compliance controller is presented. The experimental implementation of a multi-dimensional compliance case (adaptive model reference compliance controller shown in Figure 1 (b)), is discussed. The scheme here is based on our previous work, however, the control scheme has been suitably modified to improve multi-variable control performance ([15,16] and to compute the external forces/troques by separating it from an estimate of the robot's own body torques (mainly the gravitational torques). An adaptive multi-dimensional compliance model reference adaptive controller is implemented in real-time on 4 DOFs of the humanoid BERT II arm in Cartesian space (see Figure 1 (a)). The robot manipulator is controlled in such a way as to follow the compliant passive behaviour of a reference mass-spring-damper system model subject to externally sensed forces/torques in all DOFs in contrast to the one dimensional version [16]. The relevant reference model converts all measured torques into their equivalent forces at the end-effector and reacts accordingly. The suggested control scheme takes particular account of the multi-variable aspect and the problem of the robot body's own torques when measuring external torques. The redundant DOFs were used to control the robot motion in a human-like pattern via effort minimisation in the same manner as [16]. Similarly, associated actuator saturation issues were addressed by incorporating the novel AW-compensator. Moreover, the control scheme presented by [8] is adjusted to allow for a more versatile set of controller parameters suited to the multi-variable control problem of multi-redundant robots. This modified scheme employs dynamically changing forgetting factors introduced into the adaptive laws (details can be found in our work [15]).

2.1. *Adaptive Compliance Control*

In general, model free adaptive controllers are easy to implement and can minimize computational issues. To implement such controllers, almost no information about the parameters of the robots is necessary. Only the general structure of the model which consists of the inertia matrix, coriolis/centripetal vector and the gravity vector is considered. One such a controller is the powerful adaptive compliance controller developed by Colbaugh et *al.* [8]; it has been employed and extended here by

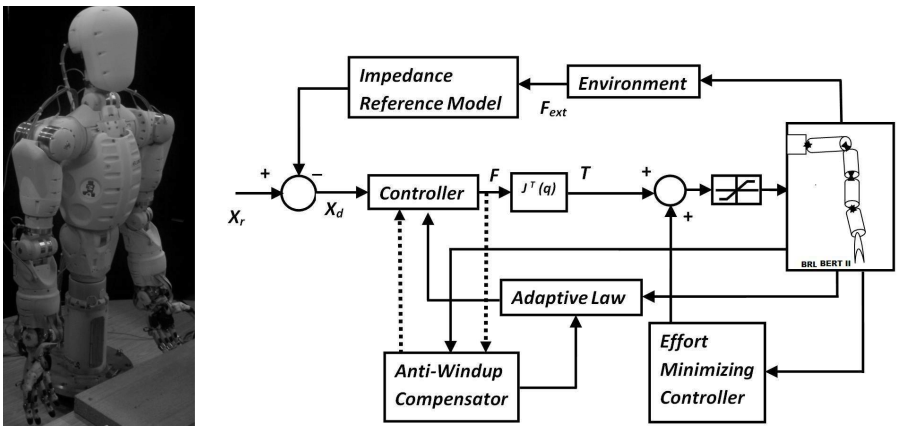

(a) (b)

Fig. 1: (a) BRL BERT II torso with two arms and hands (b) MRAC based Adaptive compliance scheme with Anti-windup compensator and posture controller[16,15,8,7,9] .

an AW-compensation scheme, while the controller scheme has been suitably modified to improve multi-variable control performance. Motivations for this method are its ease of implementation for a higher DOF system as well as the fact that it has been developed directly in the task space. We assume the general structure of the robot dynamics is given by:

$$M(q)\ddot{q} + V(q,\dot{q}) + G(q) = T \tag{1}$$

where M is the inertia matrix, a function of the n joint angles q. V is the coriolis/centripetal vector, which also represents viscous and nonlinear damping. G is the gravity vector. Note that any practical robot is subject to friction and damping which makes it an open loop stable system. T is the input torque. The Cartesian space dynamics are now given as follows: Instead of joint torques, the dynamics equate to the forces, acting on the end effector:

$$A(q)\ddot{X} + \mu_{cc}(q,\dot{q}) + f(q) = F \tag{2}$$

where $A = (JM^{-1}J^T)^{-1}$, $\mu_{cc} = \bar{J}^T V - A\dot{J}\dot{q}$, $f = \bar{J}^T G$, $F = \bar{J}^T T$ and X is the robot end-effector Cartesian position, i.e. $X = [x, y, z]^T$, and J is the Jacobian of the kinematics $X = h(q)$, i.e.

$$J = \frac{\delta X}{\delta q} \tag{3}$$

Hence, the Cartesian velocities are defined as $\dot{X} = J\dot{q}$. The matrix $\bar{J}$ is the inertia weighted pseudo Jacobian inverse adopted from [18], (see also [24]) :

$$\bar{J} = M^{-1}J^T(JM^{-1}J^T)^{-1} \tag{4}$$

The Cartesian position of the end effector is used here to define the motion task of the robot. Hence, the dynamics of (2) represent here the Cartesian or Task dynamics. The adaptive Cartesian/task control law is:

$$F = \hat{A}\ddot{X}_d^* + \hat{B}\dot{X}_d^* + \hat{f} + F_{ext} + [2k + \hat{K}]r \tag{5}$$

where, $\hat{A}$, $\hat{B}$, $\hat{f}$ and $\hat{K}$ are adaptive gains given later, while k is a positive scalar constant chosen by the designer. Moreover, the modified velocity and acceleration error are given by $\dot{X}_d^{\ *} = \dot{X}_d + \Lambda e_x$ and $\ddot{X}_d^* = \ddot{X}_d + \Lambda \dot{e}_x$ respectively. The Cartesian position error is given by $e_x = X_d - X$, where X_d the Cartesian demand position derived from a reference model, to be discussed later. The demand position X_d is the result of the reference model discussed later in this section. The vector r is the filtered error and is defined as:

$$r = \dot{e}_x + \Lambda e_x \tag{6}$$

and Λ is a 3×3 diagonal matrix with positive values. The adaptive control laws are given by: The adaptive law estimating the gravity vector is given as:

$$\dot{\hat{f}} = -K_{\alpha_1}\hat{f} + K_{\beta_1} r \tag{7}$$

The inertia matrix in Cartesian coordinates is estimated in:

$$\dot{\hat{A}} = -K_{\alpha_2}\hat{A} + K_{\beta_2} r(\ddot{X}_d^*)^T \tag{8}$$

Coriolis/Centripetal forces are indirectly estimated via the matrices $\hat{B}$ and $\hat{K}$:

$$\dot{\hat{B}} = -K_{\alpha_3}\hat{B} + K_{\beta_3} r(\dot{X}_d^*)^T \tag{9}$$

$$\dot{\hat{K}} = -K_{\alpha_4}\hat{K} + K_{\beta_4} r r^T \tag{10}$$

and using the following dynamically changing forgetting factor:

$$K_{\alpha_i} = K_{\alpha_{i0}} + K_{\alpha_{i1}}||\dot{X}||$$

with the assumption that K_{β_i}, $K_{\alpha_{i0}}$ and $K_{\alpha_{i1}}$ are positive definite diagonal matrices. Note the minor but practically important difference of using diagonal gains for the adaptation laws in difference to [8]. This allows for better tracking of multi-variable control performance in contrast to [8].
The applied torque for adaptive control is:

$$T = J^T F,$$

which is sufficient to control the Cartesian/task dynamics (2). Nevertheless, the dynamics of (2) represent only three degrees of freedom and other control terms have to be augmented to retain stability of the other $(n-3)$ degrees of freedom, representing the posture or null-space dynamics in relation to the task dynamics.

The reference impedance model characteristics are defined by the mass matrix M_s, the damping coefficient matrix C_s and the stiffness coefficient matrix K_s. These values determine the behaviour of the reference model:

$$M_s\ddot{X}_d + C_s\dot{X}_d + K_s X_d = -F_{ext} + M_s\ddot{X}_r + C_s\dot{X}_r + K_s X_r \tag{11}$$

where, F_{ext} is the external Cartesian forces sensed through the joint torque sensors , X_r is the reference trajectory and X_d is the new demand to compensate the external force. Hence, M_s, C_s and K_s can be used to adjust the level of compliance, e.g. if K_s is decreased, the robot becomes more compliant.

Note that the simplicity of the adaptive controller (5)-(10), which does not require the structural knowledge of the inertia matrix, the coriolis force or the gravity vector, resulting in the rather simple structure of the adaptation laws, avoiding any of the geometric nonlinearities of robotic systems. Hence, the controller is (almost) model free. As the main control approach is applied to a multi-redundant system, the motion is under-constrained, and some links may follow bounded but seemingly random trajectories for a Cartesian demand position. Therefore, a posture torque controller has been added which deals with the redundant motion, to generate a human like movement pattern by minimizing the effort (a function of gravity) during reaching to a particular point in the robot work space. The method here is adopted from previous work by [29,30] (see also [11]). The 'posture' controller T_p is in the null space of the adaptive Cartesian controller, hence, it does not affect the main controller:

$$T = J^T F + N^T T_p, \; N^T = (I - J^T \hat{\bar{J}}^T) \tag{12}$$

where I is the identity matrix. $\hat{\bar{J}}$ is the preliminary estimate of the inertia weighted pseudo Jacobian inverse:

$$\hat{\bar{J}} = \hat{M}^{-1} J^T (J \hat{M}^{-1} J^T)^{-1} \tag{13}$$

with $\hat{M}$ being an estimate of the inertia matrix M (1). The posture torque, T_p is defined as:

$$T_p = -K_p \frac{\delta U_p}{\delta q} - K_d \dot{q} \tag{14}$$

where, K_p and K_d are proportional and derivative gains respectively. U_p is the 'muscle' effort function defined as:

$$U_p = G^T (K_m)^{-1} G \tag{15}$$

and G is the gravitational vector term from equation (1), and K_m is the actuator activation matrix, having positive diagonal elements.

Note that equation (13) uses an estimate of the inertia matrix $\hat{M}$. Since this is done for the posture torque controller, a good estimate for $\hat{M}$ in (13) is sufficient to gain robust and acceptable posture control performance. In the Cartesian space, the adaptive law (5) is required for better tracking accuracy.

2.2. *Anti-Windup Compensator*

Due to the highly dynamic character of the adaptive control scheme, actuators can become saturated. This has shown to cause windup of the adaptation algorithms

(7)-(10) causing destabilization of the robot controller, creating a highly unsafe environment for humans. Hence, a suitable avoidance of the windup of the adaptation algorithms guarantees the controller performance in case of saturation. Another important aim is to recover nominal adaptive control performance, once the actuator saturation is overcome. Therefore, an AW compensator system is adopted from [13], originally developed for a neural network control scheme. Two functions $DZ_{K_f}(||F||)$ and $c(DZ_{K_f}(||\bar{F}||))$ are introduced for this anti-windup compensator:

$$DZ_{K_f}(||F||) = \begin{cases} ||F|| - K_f, \, if||F|| > K_f \\ 0, \qquad if||F|| \leq K_f \end{cases} \tag{16}$$

K_f is the artificial limit, imposed on the control signal. The function $c(\cdot)$, $0 \leq c \leq 1$ is a smooth scheduling element defined as follows,

$$c(DZ_{K_f}) = \frac{K_f^2 \delta}{(K_f + DZ_{K_f})(K_f \delta + DZ_{K_f})} \tag{17}$$

where δ is a positive design constant. The purpose of the scheduling element c is to activate a sliding mode element when actuator saturation is foreseen due to large amplitudes in F. When $c = 1$, only the adaptive controller is active and if $c = 0$, only a sliding mode control is active. If $0 < c < 1$, both adaptive and sliding mode controllers are active, each at a reduced level. Using $c(DZ_{K_f}(||F||))$ and $DZ_{K_f}(||F||)$ the adaptation laws for $\hat{A}$, $\hat{B}$, $\hat{f}$ and $\hat{K}$ are modified online. The adaptive law estimating the gravity forces becomes then:

$$\dot{\hat{f}} = -K_{\alpha_1} \hat{f} + K_{\beta_1} cr \tag{18}$$

Similarly, the adaptive law estimating the inertia matrix is modified to:

$$\dot{\hat{A}} = -K_{\alpha_2} \hat{A} + K_{\beta_2} cr(\ddot{X}_d^*)^T \tag{19}$$

$$\dot{\hat{B}} = -K_{\alpha_3} \hat{B} + K_{\beta_3} cr(\dot{X}_d^*)^T \tag{20}$$

$$\dot{\hat{K}} = -K_{\alpha_4} \hat{K} + K_{\beta_4} crr^T \tag{21}$$

Equation (20) and (21) are the modified form of the adaptive laws indirectly estimating coriolis/centripetal forces while the forgetting factors are modified to:

$$K_{\alpha_i} = K_{\alpha_{i0}} + K_{\alpha_{i1}} ||\dot{X}|| + K_{\alpha_{i2}} DZ_{K_f} \tag{22}$$

where $K_{\alpha_{i2}}$ are positive definite diagonal design matrices. Note that the adaptation laws of (18)-(21) are also including c in contrast to (7)-(10). This modifies for $c \to +0$ the adaptive laws into autonomous stable systems so that windup prevention is introduced, which is enhanced by the increase of the forgetting factor in (22). Using this modified adaptive law, this changes the control law to:

$$\hat{F} = cF + (1 - c) K_f \frac{r}{||r||} \tag{23}$$

and the applied torques are now:

$$T = Sat(J^T \hat{F} + (I - J^T \hat{\bar{J}}^T) T_p) \tag{24}$$

where, $Sat(\cdot)$ is the saturation function defined by the amplitude limits of the actuators and $\hat{\bar{J}}(13)$ accounts for the uncertain $\hat{M}$. The argument of the function $c(DZ_{K_f}(||F||))$ has been omitted in the equations above using only c. Note that K_f has to be chosen so that $J^T \hat{F}$ remains strictly within the linear region of $Sat(\cdot)$, considering $J^T \hat{F}$ as the argument.

2.3. *Joints Torque Sensors and Body Torque estimates*

BERT II robot arm is equipped with torque sensors in each of the joints to measure the external applied forces/torques. These sensors are strain gauges arranged in a wheatstone bridge. Torque sensors were experimentally calibrated by hanging different weights and recording voltage change. When there are no external forces/torques, the joint torque sensors measure the gravity torques $T_G \, \varepsilon \mathbb{R}^{4\times 1}$ (plus also Coriolis/centripetal torques if the robot arm is moving). However, at lower velocities, coriolis/centripetal torques will be very small as compared to gravity torques. It is necessary to compensate for these body inherent torques when measuring external torques and forces. This is achieved by posing the gravity torque as a linear parameterised expression:

$$T_G = \hat{\phi} W(q) \tag{25}$$

where $\hat{\phi} \, \varepsilon \mathbb{R}^{4\times 6}$ contains the parameter estimates depending on the robot and the sensors scale, while $W \, \varepsilon \mathbb{R}^{6\times 1}$ is the regressor function formed by the geometric nonlinearities of the robot. Thus, W is a matrix consisting of suitable sin/cos functions. The parameter matrix $\hat{\phi}$ is estimated during an initial test period using a recursive least square algorithm minimising:

$$\sum_i \parallel T_{Gi} - \hat{T}_{Gi} \parallel^2,$$

$\hat{\phi}$ is constant during normal operation. As a result, the actual body torques (T_G) and their estimates ($\hat{T}_G$) are shown in Figure 2. The standard Recursive Least Square (RLS) algorithm is employed.

The error between the sensor value and the gravity torque estimate is :

$$\Upsilon_n = T_G - \hat{\phi}_{n-1}^T W_n.$$

The RLS-algorithm is therefore:

$$\eta_n = P_{n-1} W_n (\gamma + \hat{\phi}_n^T P_{n-1} W_n)^{-1}$$

where γ, $0 < \gamma < 1$, is the forgetting factor and P is an inverse correlation matrix (initialized with a large value):

$$P_n = \gamma^{-1} P_{n-1} - \eta_n W_n^T \gamma^{-1} P_{n-1}$$

Hence, the new parameter estimate is obtained as:

$$\hat{\phi}_n = \hat{\phi}_{n-1} + \eta_n \Upsilon_n^T$$

Using this parameter estimate, the gravity torques are approximated as: $\hat{T}_G = \hat{\phi}_n^T W_n$. These estimates of the gravity torques allows differentiating of external torques T_{ext} from body-own torques of the robot: $\hat{T}_{ext} = T_{measured} - \hat{T}_G$. In fact, we are using $T_{ext} = Dz(T_{measured} - \hat{T}_G)$, where, Dz is the dead zone function, to avoid the small errors in $\hat{T}_G$ affecting T_{ext}. The external torques, T_{ext}, result from external forces, F_{ext}, acting on the end-effector of the robot in x, y and z coordinates. Thus, the external torques T_{ext} have to be mapped to these forces, F_{ext}, using the inverse of Jacobian J . Note that J is not invertible and it has been found that the pseudo Jacobian inverse [16,15] in this case gives numerically wrong results for certain poses, giving incorrect, large amplitudes for the estimated values F_{ext}. Similarly, it was found that the damped pseudo-inverse:

$$J_{pseudo}^{-1} = J^T(JJ^T + \rho^2 I)^{-1}$$

, also gives large errors when computing, F_{ext} in some cases. The most suited approximate inverse in our case is the inverse using singular value decomposition (SVD):

$$J = USV^T,$$

where U and V are unitary (possibly non square) matrices and S is a matrix, where only the diagonal values are nonzero, holding *only* the non-negative singular values of J. The SVD based Jacobian inverse is:

$$J_{SVD}^{-1} = VS^{-1}U^T.$$

Hence, the estimated external end-effector Cartesian forces are:

$$F_{ext} = J_{SVD}^{-T} T_{joints}$$

2.4. *Stability*

Stability of the closed loop system can be shown here using the proof of [8] and [13] and a passivity argument. Thus, a detailed proof is avoided providing here only a short motivational explanation explanation: As in [13], the robust sliding mode control component in equation (23) replaces the adaptive component $\bar{F}$ when the saturation limit for $\bar{F}$ has been reached, i.e. for $c(\cdot) = 0$. In this case, the adaptation laws (7)-(10) are disabled avoiding windup. The increased forgetting factor of (22) guarantees that the adaptive control law decreases its amplitude so that normal operation is recovered. The adaptive compliance controller with posture torque controller and AW compensator given by (14) and (18)-(24) is locally stable and achieves an ultimately bounded tracking error. The posture torque controller is subject to a static control scheme.

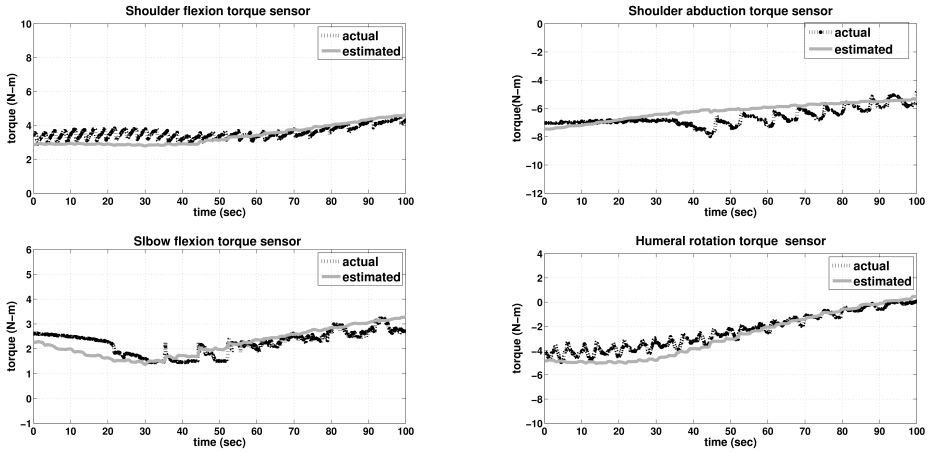

Fig. 2: Estimates of robot arm's body-own torques , T_G, $\hat{T}_G$ (real experiment).

The anti-windup compensator significantly enlarges the region of attraction of the control system in contrast to the adaptive control scheme, which destabilizes, once the control signal is saturated due to the adaptive control scheme. This is avoided by introducing an amplitude limited sliding mode element which replaces the adaptive scheme until the magnitudes of $\hat{f}$, $\hat{A}$ and $\hat{K}$ have recovered to smaller values.

3. Results and Discussion for the Compliance Controller

The controller is implemented for 4 DOF namely, shoulder flexion, shoulder abduction, humeral rotation and elbow flexion of the BERT II arm. The base coordinate frame is fixed in the shoulder. The end effector position is specified with respect to the base frame.

3.1. *Compliance Results*

In the absence of external forces, the robot end-effector should follow the reference trajectory X_r. In the presence of external contact forces the reference trajectory is modified for X_d and the robot will follow this new demand trajectory defined by the second order mass-spring-damper impedance reference model to compensate for the external forces.

The MRAC-approach allows us to design well-defined levels of compliance for safe human-robot interaction by choosing the correct values for the parameters K_s and C_s for $x - y - z$ direction. Thus, it is tested for different stiffness and damping values imposed via the model reference (second order mass-spring-damper system), for external contact forces.

These compliance results have been produced experimentally when external forces in $x - y - z$ were applied by pushing and pulling the robot end-effector while using different values of K_s and C_s (Two different experiments are shown in Figure 3 (a) and (b)). The end-effector trajectory follows the demanded reference model trajectory nicely (see also [14]).

3.2. *Anti-windup Compensator results*

Practical tests have shown that without an AW compensator, actuator amplitude limits of $\pm 3000mA$ are reached and the control system becomes easily unstable. Inclusion of the AW compensator prevents instability due to saturation. As mentioned previously, the scheduling element $c = 1$ means that the adaptive scheme is only active (see equation (23)). If $c = 0$, the sliding mode element alone is active, if $0 < c < 1$, then both the sliding mode and the adaptive controller are active.

For the real robot, it is seen that the adaptive controller is operating for most of the time, while the sliding mode scheme is only used over a short span of time when any of the actuators reaches its amplitude limit. This is particularly observed in Figure 4 for the scheduling element c which remains most of the time at $c = 1$. Hence, the AW scheme is effective, avoiding instability due to saturation but also recovering the nominal adaptive controller performance. Figure 4 also shows the motor current inputs of the humeral rotation joint and the shoulder flexion joint, which stay within the actuator amplitude limits of $\pm 3000mA$. The other two actuators (elbow flexion and shoulder abduction) are not shown, as in this experiment, their amplitude remained well below their amplitude limit. Note that this AW scheme also adds to the safety of the control scheme as it allows for the adaptive scheme to operate in the nominal case, while the AW scheme returns control to the case without saturation as quickly as possible, avoiding stability and performance loss in case of actuator saturation.

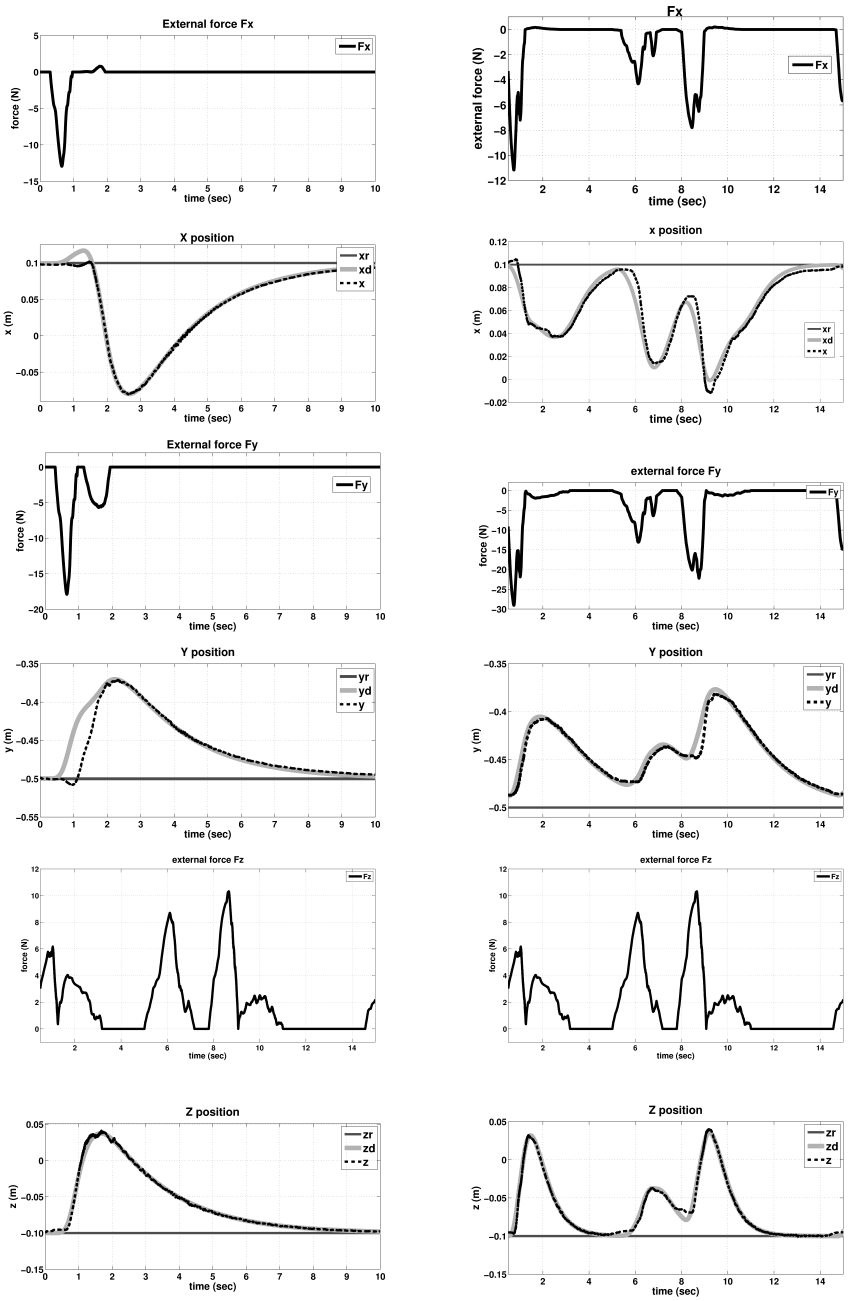

(a) (b)

Fig. 3: Cartesian position x, y and z, when external contact forces act for $K_{sxz} = 10N/m$, $C_{sxz} = 20Ns/m$, $K_{sy} = 20N/m$, $C_{sy} = 40Ns/m$ and with $M_{sxyz} = 2Kg$ (Real robot experiment Figure (a)) while, $K_{sxz} = 50N/m$, $C_{sxz} = 30Ns/m$, $K_{sy} = 30N/m$, $C_{sy} = 100Ns/m$) and with $M_{sxyz} = 2Kg$ (Real robot experiment, Figure (b).

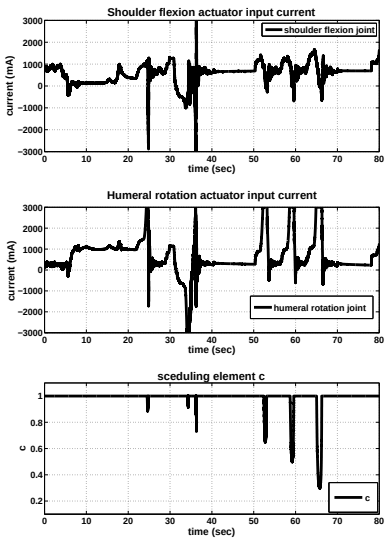

Fig. 4: Shoulder flexion and humeral rotation joint input currents are pushed to stay inside the actuator amplitude limits, scheduling element $c(\cdot)$ is also shown.

4. HRI-Example Using Compliance

Cooperative Human-human interaction features a range of communication methods which, due to their partial redundancy, help to make interaction in diverse, noisy and chaotic environments possible. With the emergence of robotic carers or other robotic assistance, which will operate with or close to humans, it will be desirable that such robots are equipped with similar communication and sensing capabilities as humans. This will not only allow the human to interact 'naturally' with the robot, but also will contribute, due to the communication and sensing redundancy, to safety during interaction.

Here, we present an integrated system which has been successfully employed in a safe object passing task between a human and a robot. The system consists of (i) an anthropomorphic hand, comprising capabilities like grasping, pointing, releasing and 'sensitive' hand-over [22,23] (see section 4.2); (ii) a humanoid robot arm fitted with a model reference adaptive compliance controller with contact detection, running on a dSPACE system; (iii) a bi-directional spoken language interface to issue commands, report states and request instructions [22,23] (see Section 4.3). We show how those subsystems, all running on different computational platforms, can be integrated, and demonstrate the system's functionality with an interaction scenario that utilises all (built in) modalities.

Fig. 5: BERT II arm hands a cup to a human experimenter.

4.1. *Interaction Scenario*

For the experimental work presented here, we have designed a simplified human-robot interaction scenario. Although this only demonstrates a small aspect of human-robot interaction that would be desirable in future care robots, it is representative for situations where a robot assists a physically less-able and possibly bedridden human.
Imagine the following care situation: A bedridden human should be able to direct the robot towards a set of locations and instruct the robot to perform a certain task at a given location. During the repositioning of the robot, collisions can occur and the robot would need to be able to sense those, reduce the impact force to a minimum, report the collision to the human and ask for advice on how to proceed. Handling tasks that the robot performs should also be sensitive to impact. The hand-over of objects is of particular importance and the robot would be required to only release objects when the human holds them firmly.

Our simplified lab scenario reflects this general purpose example. A human is placed at a chair and the BERT II (see the work by Lenz et al. [23]) robot arm is mounted on a stand. A paper bin is placed out of reach of the human but within reach of the robot (see Figure 5). The robot arm can extend its hand to the human. In our scenario, two locations (i.e. 'close to human' and 'above bin') are pre-programmed, but could easily be dynamically set or acquired by a higher level perception and reasoning system, as reported by Lallee et *al.* [22]. The human can now verbally instruct the robot to move to him/her or to the bin. Furthermore, it is possible to instruct the robot to take an object, release an object or hand-over an object. The difference between release and handover is that in the former the robot hand simply opens, whereas in the latter the hand opens only when the hand's

sensing system perceives firm human contact with the handled object. During all those interactions, the robot also verbally announces its next action and position, which raises the human's awareness and therefore also enhances safety.

During the arm motion, the adaptive controller dynamically estimates the torques in the arm, which are subject to joint angles, velocities and accelerations. If the measured torque exceeds the body-own torque by a threshold torque, a collision is assumed. The robotic system verbalises this to the human and waits for further instructions. The human can then either instruct the robot to stay were it is or alternatively return to the last established position before a motion command was issued. This introduces an important safety feature in addition to the active compliance of the robot arm.

4.2. *Grasping Controller for an Anthropomorphic Hand*

For the grasping of objects, a single anthropomorphic hand module (Figure 6) has been integrated into the arm control infrastructure [22,23,17]. The hand has nine DOF comprising gross movement for all 5 fingers, "trigger" action for index and middle finger, opposing of the thumb, and finger spread. Each DOF is actuated by a geared brushless DC motor and the lowest level motor control is established via an EPOS 24/1 positioning controller.

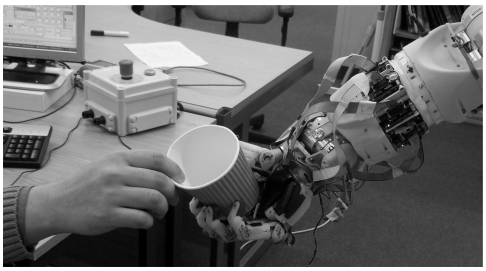

Fig. 6: The BERT II anthropomorphic hand (right) during an object hand-over procedure.

4.3. *Spoken Language Interface and High Level Control*

In order to enable spoken language interaction we have integrated the CSLU Toolkit ([32]) Rapid Application Development (RAD) into the arm control infrastructure [17]. YARP based interface [12] has been used together with the dSPACE to communicate and translate speech command into motor commands.

The BERT II robot arm was controlled via the model reference adaptive controller (MRAC) shown in Figure 1 (b) (see also [16,15]) described in Section 2. As mentioned before, the reference model is a compliant, second order mass-spring

damper system, the stiffness and damping terms can be selected to achieve several different compliance characteristics. The arm controller employed 4 joints, namely shoulder flexion, humeral rotation, elbow and wrist flexion joints (same as in Section 2). The adaptive controller was used in this experiment because of the unknown dynamics of the arm as well as the nature of the application, i.e. the handover process between human and robot, which cannot rely on a fixed dynamic model.

Our controller operates in Cartesian space (x, y and z) which only requires 3 DOF as reported in Section 2. The redundant 4th DOF is therefore utilised to generate human like motion in the arm by employing an effort minimizing posture controller based on the work of [29,30]. The overall control scheme for the BERT II arm is shown in Figure 1 (b).

4.4. *Results and Discussion*

Figure 7 shows the verbal communication, arm motions and recorded forces during the interaction. BERT II asks the human what the next action should be, reports

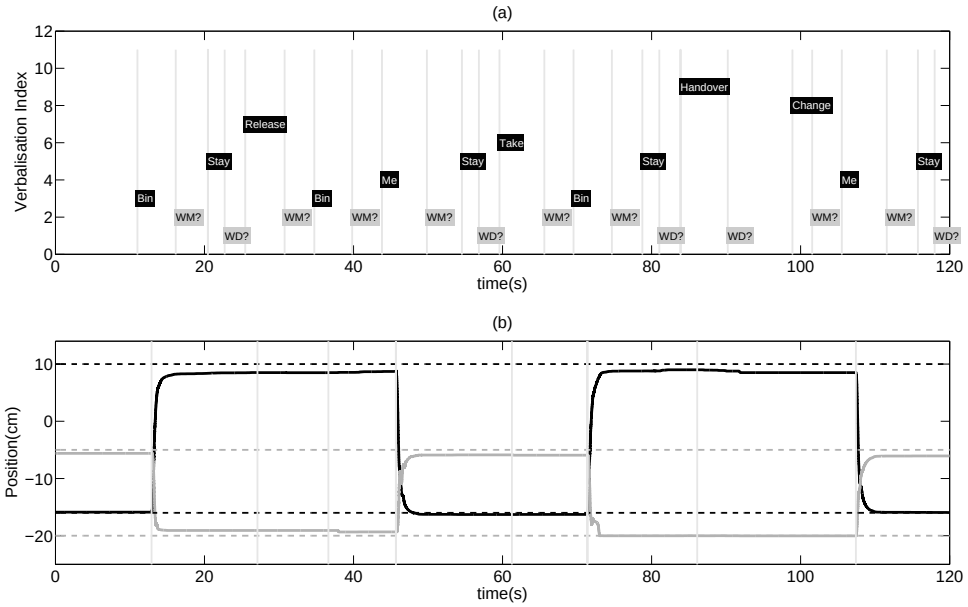

Fig. 7: Illustration of interaction scenario: (a) shows the verbal utterances of the human (white on black) and the robot (black on grey); (b) shows the robot arm motion as a consequence of the verbal communication in Cartesian coordinates. The black line represents the x-direction and the grey line the z-direction. The dotted lines represent the target positions. The y-direction was omitted for clarity. The grey vertical lines in (a) and (b) represent the times when verbal utterances and motor commands were issued.

its current position and the next action. The plots arranged in a synchronised way, illustrating the timing between verbal communication[a], the issuing of the motor commands and the actual motor action. The scenario illustrates how we interacted with the robot and how objects were grasped, released and transferred between locations (see also Fig. 5 and [14]).

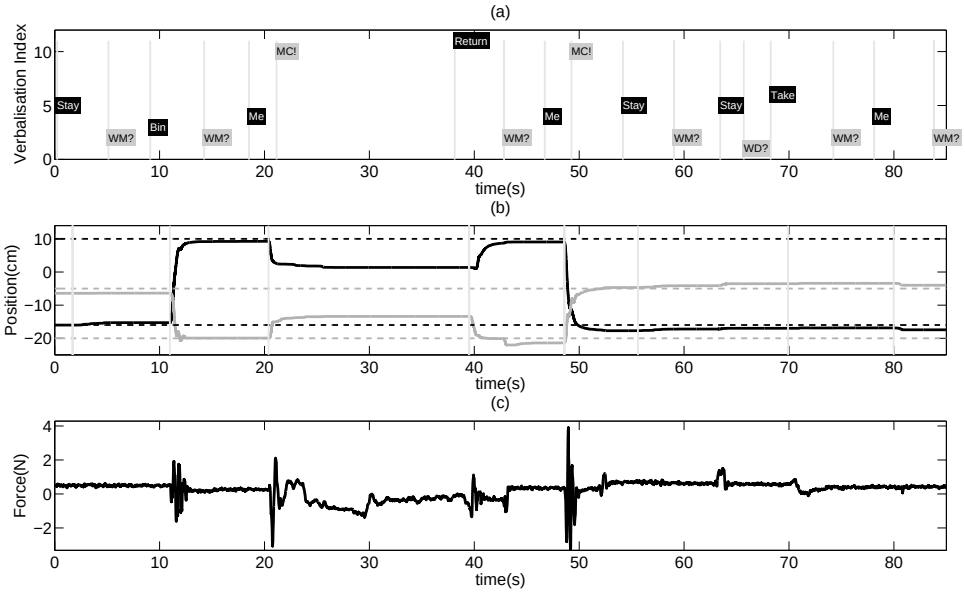

Fig. 8: Illustration of interaction scenario: (a) shows the verbal utterances of the human (white on black) and the robot (black on grey); (b) shows the robot arm motion as a consequence of the verbal communication in Cartesian coordinates. The black line represents the x-direction and the grey line the z-direction. The dotted lines represent the target positions and the y-direction was omitted for clarity; (c) shows the force acting on the robot in the z-direction during collisions. The two collision events (at $t \approx 22s$ and $t \approx 50s$) are resolved, based on the human instruction, by returning to the last position or staying at the current position respectively. The grey vertical lines in (a) and (b) represent the times when verbal utterances and motor commands were issued.

Figure 8 illustrates a collision event. For clarity, only the force acting in the z-direction is shown in Figure 8 (c). The robot reports the detected collisions verbally to the human, while the compliant controller reduces damages during the collision. The human then directs the robot to return to the last position (at $t \approx 38s$) or to

[a]Abbreviations of robot utterances used in the plots: WM?="Where should I move?"; WD?="What should I do?"; MC!="I have made contact, what should I do?"

stay where it is (at $t \approx 55s$), since in the latter case the actual position was very close to the target.

5. Conclusion

In this paper we have presented a multi-dimensional compliance control of a humanoid robot arm. The controller is an adaptive model reference compliance controller employing joint torque sensors for interaction force with environment. The compliant reference model is a second order mass-spring-damper system. The values of the spring constant and the damping coefficient can be changed to produce different levels of compliance. Associated windup/actuator saturation issues have been addressed via a novel anti-windup compensator. The scheme is dynamic model free and the redundant degree of freedom is employed to generate human-like posture. In addition, the adaptive compliance scheme is employed for a human robot interaction experiment. This shows the effectiveness of compliance in HRI. In the experiment, a human experimenter speaks with the robot and an object is passed from human to a robot arm. We have successfully demonstrated how diverse subsystems (including this model reference adaptive compliance controller) can be integrated to allow for safer human robot interaction. It is very clear that future robotic systems operating amongst humans will require advanced sensing systems (like artificial skin and high resolution finger-tip sensor) in order to successfully and safely assist humans. We have shown that even without those sensors, safety and dexterity is possible by exploiting information that can be obtained from motor currents (in case of the hand) or joint torque sensors (in case of the arm). This is not to say that more advanced sensors are not required. On the contrary, by combining advanced skin sensors with the already built-in sensing structure, future systems can be engineered for robustness, mutual enhancement and graceful degradation in the event of sub-system failure.

6. Acknowledgements

The research leading to these results has received funding from the European Community's Information and Communication Technologies Seventh Framework Programme [FP7/ 2007.2013] under grant agreement no. [215805], the CHRIS project.

References

1. M.O. Al-Jarrah and Y.F. Zheng. Intelligent compliant motion control. *IEEE Transaction on System, Man, and Cybernetics-Part B Cybernetics*, 28:116–122, Febuarary 1998.
2. C.V. Albrichsfeld, M. Svinin, and H. Tolle. Learning approach to the active compliance control of multi-arm robots coupled through a flexible object. In *Proc. of 3rd European Control Conference*, 1995.
3. C.V. Albrichsfeld and H. Tolle. A self-adjusting active compliance controller for multiple robots handling an object. *Control Engineering Practice*, 10:165–173, February 2002.

4. A. Albu-Schäffer, Haddadin, C. Ott, T. Stemmer, G. Wimbck, and Hirzinger. The dlr lightweight robot: design and control concepts for robots in human environments. *Control Engineering Practice*, 34:376–385, 2007.
5. A. Bichi and G. Tonietti. Design, realization and control of soft robot arms for intrinsically safe interaction with humans. In *Proc. IARP/RAS Workshop on Technical Challenges for Dependable Robots in Human Environments*, pages 79–87, October 2002.
6. D.J. Braun, F. Petit, F. Huber, S. Haddadin, P. van der Smagt, A. Albu-Schaffer, and S. Vijayakumar. Robots driven by compliant actuators: Optimal control under actuation constraints. *Robotics, IEEE Transactions on*, 29(5):1085–1101, 2013.
7. R. Colbaugh, K. Glass, and K. Wedeward. Adaptive compliance control of electrically-driven manipulators. In *Proceedings of the 35th Conference on Decision and Control*, pages 394–399, Kobe,Japan, December 1996.
8. R. Colbaugh, H. Seraji, and K. Glass. Adaptive compliant motion control for dextrous manipulators. *The International Journal of Robotic Research*, 14(3):270–280, 1995.
9. R. Colbaugh, K. Wedeward, K. Glass, and H. Seraji. New results on adaptive compliant motion control for dextrous manipulators. *The International Journal of Robotic and Automation*, 11(1), 1996.
10. Franois Conti, Jaeheung Park, and Oussama Khatib. Interface design and control strategies for a robot assisted ultrasonic examination system. In O. Khatib, V. Kumar, and G. Sukhatme, editors, *Experimental Robotics*, volume 79 of *Springer Tracts in Advanced Robotics*, pages 97–113. Springer Berlin Heidelberg, 2014.
11. V. De Sapio, O. Khatib, and S. Delp. Simulating the task level control of human motion: a methodology and framework for implementation. *The Visual Computer*, 21(5):289–302, 2005.
12. P. Fitzpatrick, G. Metta, and L. Natale. Towards long-lived robot genes. *Robot. Auton. Syst.*, 56(1):29–45, 2008.
13. G. Herrmann, M.C. Turner, and I. Postlethwaite. Performance-oriented antwindup for a class of linear control systems with augmented neural network controller. *IEEE Transactions on Neural Networks*, 18(2):449–465, March 2007.
14. S.G. Khan and G. Herrmann. https://www.youtube.com/watch?v=ike8rrtr-ow, 2014.
15. S.G. Khan, G. Herrmann, T. Pipe, and C. Melhuish. Adaptive multi-dimensional compliance control of a humanoid robotic arm with anti-windup compensation. In *Intelligent Robots and Systems (IROS), 2010 IEEE/RSJ International Conference on*, pages 2218 –2223, 2010.
16. S.G. Khan, G. Herrmann, T. Pipe, C. Melhuish, and A. Spiers. Safe adaptive compliance control of a humanoid robotic arm with anti-windup compensation and posture control. *International Journal of Social Robotics*, 2:305–319, 2010.
17. S.G. Khan, A. Lenz, G. Herrmann, T. Pipe, and C. Melhuish. Towards safe human robot interaction: Integration of compliant control, an anthropomorphic hand and verbal communication. In *FIRA 2011 Conference: ICAHRR*, Taiwan, 2011.
18. O. Khatib. A unified approach for motion and force control of robot manipulators: The operational space formulation. *IEEE Jounrnal of Robotics and Automation*, RA3(1):43–53, 1987.
19. B. Kim, S. Oh, h. Suh, and B. Yi. A compliance control strategy for robot manipulators under unknown environment. *KSME International Journal*, 14:1081–1088, February 2000.
20. S. Komada and K. Ohnishi. Robust force and compliance control of robotics manipulators. In *Proceedings of the International Conference on Industrial Electronics*, Hyatt Regency, Singapore, October 1988.

21. Dominic Lakatos, Gianluca Garofalo, Florian Petit, Christian Ott, and Alin Albu-Schäffer. Modal limit cycle control for variable stiffness actuated robots. In *ICRA*, pages 4934–4941, 2013.
22. S. Lallée, Séverin L., A. Lenz, C. Melhuish, L. Natale, S. Skachek, T. Van Der Zant, F. Warneken, and P. F. Dominey. Towards a platform-independent cooperative human-robot interaction system: I. perception. In *IROS IEEE/RSJ International Conference on Intelligent Robots and Systems*, 10-2010 2010.
23. A. Lenz, S. Skachek, K. Hamann, J. Steinwender, A.G. Pipe, and C. Melhuish. The BERT2 infrastructure: An integrated system for the study of human-robot interaction. In *Humanoid Robots (Humanoids), 2010 10th IEEE-RAS International Conference on*, pages 346–351, 2010.
24. B. Nemec and L. Zlajpah. Null space velocity control with dynamically consistent pseudo-inverse. *Robotica*, 18(1):513518, 2000.
25. C. Ott, A. Albu-Schäffer, A. Kugi, and G. Hirzinger. Decoupling based cartesian impedance control of flexible joint robots. In *Proceedings of the IEEE International Conference on Robotics and Automation*, Taipei, Taiwan, 2003.
26. Z. Peng and N. Adachi. Compliant motion control of kinematically redundant manipulators. *IEEE Transactions on Robotics and Automation*, 9:831–837, Febuarary 1993.
27. B.R. Shetty and M.H. Ang. Active compliance control of a puma 560 robot. In *Proceedings of the IEEE International Conference on of Robotics and Automation*, Minneapolis, Minnesota, Canada, 1996.
28. J.J.E. Slotine and W. Li. *Applied Nonlinear Control*. Pearson Prentice Hall, Upper Saddle River, NJ, USA, 1991.
29. A. Spiers, G. Herrmann, and C. Melhuish. Implementing discomfort in operational space: Practical application of a human motion inspired robot controller. *TAROS conference: Towards Autonomous Robotic Systems*, August 2009.
30. A. Spiers, G. Herrmann, C. Melhuish, T. Pipe, and A. Lenz. Robotic implementation of realistic reaching motion using a sliding mode/operational space controller. *Lecture Notes in Computer Science (ICSR '09)*, pages 230–238, 2009.
31. Adam Stokes, Robert F. Shepherd, Stephen A. Morin, Filip Ilievski, and George M. Whitesides. A hybrid combining hard and soft robots. *Soft Robotics*, 2013.
32. S. Sutton, R. Cole, J. De Villiers, J. Schalkwyk, P. Vermeulen, M. Macon, Y. Yan, E. Kaiser, B. Rundle, K. Shobaki, P. Hosom, A. Kain, J. Wouters, D. Massaro, and M. Cohen. Universal speech tools: The cslu toolkit. In *In the Proceedings Of The Intenational Conference On Spoken Language Processing (ICSLP)*, volume 7, pages 3221—3224, 1998.
33. T. Tsumugiwa, R. Yokogawa, and K. Hara. Variable impedance control based on estimation of human arm stiffness for human-robot cooperative calligraphic task. In *Proceedings of the IEEE International Conference on Robotics*, pages 644–650, Washington,USA, May 2002.
34. Milos Vasic and Aude Billard. Safety Issues in Human-Robot Interactions. In *Proceedings of the 2013 IEEE-RAS International Conference on Robotics and Automation*, 2013.
35. A. Vick, D. Surdilovic, and J. Kruger. Safe physical human robot interaction with industrial dual arm robots. In *Proceedings of the 9th International Workshop on Robot Motion and Control, Poland*, pages 264–269, 2013.
36. Luigi Villani, Hamid Sadeghian, and Bruno Siciliano. Null-space impedance control for physical human-robot interaction. In Vincent Padois, Philippe Bidaud, and Oussama Khatib, editors, *Romansy 19 Robot Design, Dynamics and Control*, volume 544 of

CISM International Centre for Mechanical Sciences, pages 193–200. Springer Vienna, 2013.

37. W. Zhang, Q. Huang, P. Du, J. Li, and K. Li. Compliance control of a humanoid arm based on forced feedback. In *Proceedings of the 2005 IEEE International Conference on Information Acquisition*, Hong Kong and Macau, China, July 2005.
38. L. Zollo, Siciliano B., C. Laschi, G. Teti, and P. Dario. An experimental study on compliance control for a redundant personal robot arm. *Robotics and Autonomous Systems*, 44:101–129, 2003.